Int. J. Heat Mass Transfer. Vol. 35, No. 12, pp. 3419–3429, 1992
Printed in Great Britain

0017–9310/92 $5.00 + 0.00

Effects of film evaporation on laminar mixed convection heat and mass transfer in a vertical channel

WEI-MON YAN
Department of Mechanical Engineering, Hua Fan Institute of Technology, Shih Ting, Taipei, Taiwan 22305, R.O.C.

(*Received* 26 *August* 1991 *and in final form* 13 *December* 1991)

Abstract—A numerical study of finite liquid film evaporation on laminar mixed convection heat and mass transfer in a vertical parallel plate channel is presented. The influences of the inlet liquid mass flow rate and the imposed wall heat flux on the film vaporization and the associated heat and mass transfer characteristics were examined for air–water and air–ethanol systems. Predicted results obtained by including transport in the liquid film are contrasted with those where liquid film transport is neglected, showing that the assumption of an extremely thin film made by Tsay and Yan (*Wärme- und Stoffübertragung* **26,** 23–31 (1990)) is only valid for a system with a small liquid mass flow rate. Additionally, it is found that the heat transfer between the interface and gas stream is dominated by the transport of latent heat associated with film evaporation. The magnitude of the evaporative latent heat flux may be five times greater than that of sensible heat flux.

1. INTRODUCTION

HEAT AND mass transfer are important in processes such as evaporative cooling for waste heat disposal, cooling of a high temperature surface by coating it with a phase-change material, liquid film evaporators, turbine blade cooling, combustion premixing, distillation of a volatile component from a mixture with involatiles, double-diffusion convection in ocean flows and the simultaneous diffusion of metabolic heat and perspiration in controlling our body temperature, especially on a hot summer's day. With the channel wall being wetted by a thin liquid film, great augmentation in heat transfer can be expected because of the simultaneous presence of two buoyancy forces—thermal and mass diffusion buoyancy forces. One results from the density non-uniformity due to a temperature gradient and the other due to a concentration gradient in conjunction with film vaporization, which causes the transfer of latent heat. This study aims to examine the effects of combined thermal and solutal buoyancy forces on laminar mixed convection heat and mass transfer between vertical parallel plates with film evaporation.

Mixed convection heat transfer in vertical channel flows influenced by thermal buoyancy force alone has been studied in great detail [1–5]. Coupled heat and mass transfer over flat plates with different inclinations or along vertical cylinders and cones in natural convection flows has been the subject of many papers [6–9]. Recently, natural convection heat and mass transfer in vertical channels has been widely studied by Lee *et al.* [10] and Yan and Lin [11, 12]. Yan and Lin [11, 12] found that heat transfer is greatly enhanced due to the presence of solutal buoyancy force. For forced convection heat and mass transfer, studies have been carried out for flows over a flat plate [13, 14] and a wedge [15]. As far as mixed convection heat and mass transfer is concerned, Yeh *et al.* [16] numerically examined the effects of heat and mass buoyancy forces on laminar forced convection heat transfer over a flat plate. Recently, Yan and coworkers [17–19] investigated the influences of a wetted wall on laminar mixed convection heat transfer in vertical ducts. As in the case of natural convection heat and mass transfer [11, 12], the heat transfer enhancement through mass diffusion connected with film vaporization is pronounced.

Due to the complicated couplings between momentum, heat and mass transfer in gas stream and momentum and heat transfer in the liquid film through their common interface, the studies [11–19] just reviewed above all focused their attention on heat and mass transfer in the gas stream, with the neglect of the liquid film thickness. The results thus produced are only good for systems having an extremely thin film thickness. However, in practical situations, the liquid film along the channel wall is of finite thickness, and thereby the effects of the momentum and energy transport in the liquid film on the heat and mass transfer in the flowing gas should be considered in the analysis. In this connection, the effect of liquid film on the forced convection heat and mass transfer in a gas stream has been treated in some studies [20-22]. In these studies, a Nusselt type approximation was adopted to simplify the treatment of transport in liquid film. Additionally, the effects of buoyancy forces of thermal and mass diffusion on the heat and mass transfer are not considered in their analyses. The evaporative cooling of the liquid film falling along a

NOMENCLATURE

B	liquid mass flow rate per unit periphery length at inlet
b	channel width
c_p	specific heat
D	mass diffusivity
Gr_T	Grashof number (heat transfer), $gq''_w b^2/(v_0^2 \cdot k_0)$
g	gravitational acceleration
h_{fg}	latent heat of evaporation
h_M	mass transfer coefficient, equation (24)
k	thermal conductivity
M_r	dimensionless accumulated evaporation rate, equation (29)
$\dot{m}''_I$	interfacial mass flux
Nu_l	interfacial Nusselt number for latent heat transport, equation (23)
Nu_s	interfacial Nusselt number for sensible heat transport, equation (22)
Nu_x	overall Nusselt number, equation (21), $Nu_s + Nu_l$
p	mixture pressure
p_m	motion pressure (dynamic pressure), $p - p_0$
q''_I	total interfacial energy flux in gas side, equation (19)
q''_{Il}	interfacial latent heat flux in gas side (or net enthalpy flux), $\dot{m}''_I \cdot h_{fg}$
q''_{SI}	interfacial sensible heat flux in gas side
q''_w	wall heat flux
Re	inlet Reynolds number of gas stream
Sc	Schmidt number
Sh	interfacial Sherwood number
T	temperature
T_{l0}	inlet liquid film temperature
T_I	gas–liquid interface temperature
U	dimensionless axial velocity, u/u_0
u	axial velocity
u_0	inlet axial velocity
v	transverse velocity
W	dimensionless mass fraction of vapor, $(w - w_0)/(w_I - w_0)$
w	mass fraction of vapor
w_I	mass fraction of vapor at gas–liquid interface
x	coordinate in the flow direction
Y	dimensionless coordinate in the transverse direction, y/b
y	coordinate in the transverse direction.

Greek symbols

δ	local liquid film thickness
θ	dimensionless temperature, $(T - T_0)/(T_w - T_0)$
μ	molecular dynamic viscosity
ρ	density
τ_I	shear force at the gas–liquid interface
ϕ	relative humidity in the ambient.

Subscripts

a	air
g	mixture (air + water vapor or ethanol vapor)
I	condition at the gas–liquid interface
l	liquid
0	at ambient condition or inlet condition
v	vapor
w	condition of wall.

vertical plate or along channel walls of a vertical channel was recently explored by Yan and colleagues [23–25]. Their numerical calculation and experimental measurement indicate that the efficient heat transfer is due to the latent heat exchange associated with film evaporation. It suffices to say that in spite of wide application in practice, the mixed convection heat and mass transfer between vertical parallel plates with film vaporization is still poorly understood from the above review. This motivates the present study. The main objective of this work is to extend the previous work [17–19] to investigate the effects of finite liquid film evaporation on laminar mixed convection heat and mass transfer in a vertical channel.

2. ANALYSIS

The geometry of the problem under consideration is a vertical parallel plate channel with channel width b. The right vertical plate is heated and kept at a uniform wall heat flux q''_w. The left plate is a dry wall and is kept thermally insulated. The liquid film flows down over the right, heated vertical plate under the action of gravity with an inlet liquid temperature T_{l0} and an inlet mass flow rate B. Air at constant temperature T_0 enters the channel from the top at a constant velocity u_0. Part of the imposed wall heat flux is convected downstream by the liquid film and partly transferred across the film to the interface, where it is absorbed by the film vaporization process and lost to the gas stream through sensible heat transfer. The liquid film gets heated as it flows downstream, resulting in a rise in interfacial temperature and concentration. The thermal and solutal buoyancy forces are thus generated. Therefore, the forced gas flow in the channel is modified by these buoyancy forces along with the shearing effects created by the falling film.

In the present study a detailed numerical study was performed to investigate the mixed convection heat and mass transfer by simultaneously solving the con-

servation equations for various transport processes in the liquid film and gas stream with interfacial matching conditions treated. Thus the problem is of conjugated nature.

2.1. *Governing equations*

2.1.1. *Liquid film.* As a preliminary study, consideration is given to a system with a low liquid mass flow rate and hence the liquid film is assumed to flow laminarly. Because the film thickness in this study is about 2×10^{-4} m, it is reasonable to neglect the inertial terms in the momentum equation, as compared with the diffusional term (viscous term). Moreover, for the thin liquid film the longitudinal transfers of momentum and energy are much smaller than those in the transverse direction. With these simplifications, the steady laminar momentum and heat transfer in the liquid film can be described by the following conservation equations:

axial-momentum equation

$$0=\partial(\mu_l\,\partial u_l/\partial y)/\partial y+\rho_l g \tag{1}$$

energy equation

$$\rho_l c_{pl}u_l\,\partial T_l/\partial x=\partial(k_l\,\partial T_l/\partial y)/\partial y. \tag{2}$$

2.1.2. *Gas flow.* The steady laminar mixed convection heat and mass transfer in the gas flow can be explored, with the usual boundary-layer approximations, by the basic equations:

continuity equation

$$\partial(\rho_g u_g)/\partial x+\partial(\rho_g v_g)/\partial y=0 \tag{3}$$

axial-momentum equation

$$\rho_g u_g\,\partial u_g/\partial x+\rho_g v_g\,\partial u_g/\partial y=-\mathrm{d}p_m/\mathrm{d}x+\partial(\mu_g\,\partial u_g/\partial y)/\partial y+g(\rho_g-\rho_0) \tag{4}$$

energy equation

$$\rho_g c_{pg}u_g\,\partial T_g/\partial x+\rho_g c_{pg}v_g\,\partial T_g/\partial y=\partial(k_g\,\partial T_g/\partial y)/\partial y+\rho_g D(c_{pv}-c_{pa})(\partial T_g/\partial y)\cdot(\partial w/\partial y) \tag{5}$$

concentration equation of vapor

$$\rho_g u_g\,\partial w/\partial x+\rho_g v_g\,\partial w/\partial y=\partial(\rho_g D\,\partial w/\partial y)/\partial y. \tag{6}$$

In the study of steady mixed convection channel flow, the overall mass balance at every axial location should be satisfied:

$$\int_0^{b-\delta}\rho_g u_g\,\mathrm{d}y=\rho_0 u_0(b-\delta_0)-\int_0^x\rho_g v_I\,\mathrm{d}x. \tag{7}$$

This equation is used to deduce the pressure gradient in the gas flow.

2.2. *Boundary and interfacial matching conditions*

The boundary conditions are:

$$x=0:\quad u_g=u_0,\quad T_g=T_0,\quad T_l=T_{l0},\quad w=w_0 \tag{8}$$

$$y=0:\quad u_g=\partial T_g/\partial y=\partial w/\partial y=0 \tag{9}$$

$$y=b-\delta:\quad u_g=u_l(x),\quad u_l=u_l(x),\quad T_g=T_l(x),\quad w=w_l(x) \tag{10}$$

$$y=b:\quad u_l=0,\quad k_l\,\partial T_l/\partial y=q''_w. \tag{11}$$

The interfacial matching conditions specified at $y=b-\delta$ are described as follows:

(i) continuity of velocity

$$u_l(x)=u_{g,I}=u_{l,I}; \tag{12}$$

(ii) continuity of temperature

$$T_l(x)=T_{g,I}=T_{l,I}; \tag{13}$$

(iii) continuity of shear stress

$$\tau_I(x)=\mu_g(\partial u_g/\partial y)_I=\mu_l(\partial u_l/\partial y)_I; \tag{14}$$

(iv) transverse velocity of the air–vapor mixture is deduced by assuming that the interface is semi-permeable [26]—that is, the solubility of air in the liquid film is negligibly small and the y-directed velocity of air is zero at the interface

$$v_I=-D/(1-w_I)\cdot(\partial w/\partial y)_I; \tag{15}$$

(v) by assuming the interface is in thermodynamic equilibrium and the air–vapor mixture is an ideal gas mixture [26], the mass fraction of water or ethanol vapor at the interface can be evaluated by the relation

$$w_I=M_v p_I/[M_a(p-p_I)+M_v p_I] \tag{16}$$

where p_I is the partial pressure of vapor at the interface, and M_v and M_a are, respectively, the molar masses of vapor and air;

(vi) vaporizing flux of vapor into the gas stream is

$$\dot m''_I=\rho_g D/(1-w_I)\cdot(\partial w/\partial y)_I; \tag{17}$$

(vii) energy balance at the gas–liquid interface

$$(k\,\partial T/\partial y)_{l,I}=(k\,\partial T/\partial y)_{g,I}+\dot m''_I\cdot h_{fg} \tag{18}$$

where $\dot m''_I$ and h_{fg} are the evaporated mass flux and latent heat of vaporization respectively. It is worth noting in equation (18) that the first and second terms on the right-hand side represent the interfacial heat flux from the interface to the gas stream, q''_{SI}, and the net enthalpy due to the latent heat transfer (film vaporization), q''_{II}, respectively. The term on the left-hand side of equation (18) stands for the interfacial heat flux in the liquid side and is regarded as the interfacial heat flux q''_I. Therefore, the interfacial heat flux from the interface to the gas stream can then be expressed as

$$q''_I=q''_{SI}+q''_{II}=(k\,\partial T_g/\partial y)_{g,I}+\dot m''_I\cdot h_{fg}. \tag{19}$$

The local Nusselt number at the interface, defined as

$$Nu_x=h\cdot(2b)/k_g=q''_I\cdot(2b)/[k_g\cdot(T_I-T_b)] \tag{20}$$

can be written as

$$Nu_x=Nu_s+Nu_I \tag{21}$$

where Nu_s and Nu_l are, respectively, the local Nusselt numbers for sensible and latent heat transfer, and are defined as

$$Nu_s = (k_g \partial T_g/\partial y) \cdot (2b)/[k_g(T_i - T_b)] \quad (22)$$

and

$$Nu_l = \dot{m}_i'' \cdot h_{fg}(2b)/[k_g(T_i - T_b)]. \quad (23)$$

For a low mass transfer rate at the interface, the mass transfer coefficient h_M can be defined as

$$\dot{m}_i''(1 - w_i) = \rho_g h_M (w_i - w_b). \quad (24)$$

The local Sherwood number then becomes

$$Sh = h_M \cdot (2b)/D = \dot{m}_i'' \cdot (1 - w_i) \cdot (2b)/[\rho_g D(w_i - w_b)]. \quad (25)$$

Note that in the above formulation the thermophysical properties of the gas mixture and liquid film are considered as variable with temperature and mixture composition. They are calculated from the pure component data by means of mixing rules [27] applicable to any multicomponent mixtures. The pure component data [28, 29] are approximated by polynomials in terms of temperature. The complete details of the evaluation of these properties are available in refs. [23, 28]. Besides, it is worth noting that the entrainment of the liquid in the form of droplets into the gas stream may be important when the relative motion of the gas flow against the film is large. This process is rather complex and is neglected in this work because of a lack of adequate information.

3. SOLUTION METHOD

In view of the impossibility of obtaining an analytic solution for the non-linear coupled differential equations, the conjugate heat and mass transfer problem defined by the governing equations, equations (1)–(6), is solved by a finite difference numerical scheme. In the present study the matching conditions imposed at the gas–liquid interface, equations (14) and (18), to ensure the continuities of shear stress and heat flux are cast in backward difference for $(\partial\psi/\partial y)_g$ and forward difference for $(\partial\psi/\partial y)_l$ with ψ denoting u or T. Therefore, the governing equations in the gas flow and liquid film can be solved simultaneously.

Due to the interactions between the liquid film and the gas stream through their common interfaces, the solution for the problem can be better sought by finite difference procedures. Since the flow under consideration is of boundary-layer type, the finite difference solution for equations (1)–(6) can be marched in the downstream direction. The governing equations are expressed in terms of finite difference approximations by employing the upstream difference in the axial convection terms and the central difference in the transverse convection and diffusion terms. The resulting system of algebraic equations can be cast into a tridiagonal matrix equation, which can be efficiently solved by the Thomas algorithm [30]. For a given flow and thermal conditions, the solution procedures are briefly outlined as follows:

(1) Specify the flow and thermal conditions, T_{10}, q_w'', B, Re and ϕ.

(2) For any axial location, guess the values of $(-dp_m/dx)$ and δ.

(3) Solve the finite difference forms of equations (1) and (4) for velocities u_l and u_g.

(4) Numerically integrate the continuity equation of the gas stream for v_g

$$v_g = -\frac{1}{\rho_g}\frac{\partial}{\partial x}\int_0^y \rho_g u_g \, dy. \quad (26)$$

(5) Solve the finite difference forms of equations (2) and (5) for temperatures T_l and T_g.

(6) Solve the finite difference form of equation (6) for mass fraction of vapor w.

(7) Check the satisfaction of the overall conservation of mass in the gas flow and liquid film. If the following criteria

$$\left| \int_0^{b-\delta} \rho_g u_g \, dy - \left[\rho_0 u_0 (b - \delta_0) + \int_0^x \dot{m}_i'' \, dx \right] \right| \Big/ \rho_0 u_0 b < 10^{-4} \quad (27a)$$

and

$$\left| B - \left[\int_{b-\delta}^{b} (\rho u \, dy)_l + \int_0^x \dot{m}_i'' \, dx \right] \right| \Big/ B < 10^{-4} \quad (27b)$$

are met, then test convergence of the velocity, temperature and concentration fields. If the maximum relative errors for u, T and w between two consecutive iterations satisfy the criterion

$$|\psi_{i,j}^n - \psi_{i,j}^{n-1}|_{max}/|\psi_{i,j}^n|_{max} < 10^{-4}, \quad \psi = u, T \text{ and } w \quad (28)$$

then the solution for the current axial location is complete. Now if equation (28) is not simultaneously met, repeatedly solve the finite difference equations for u, v, T and w in gas stream and liquid film until the condition specified in equation (28) is fulfilled. If equations (27) are not satisfied, adjust $(-dp_m/dx)$ and δ and repeat procedures (2)–(7) for the current axial location.

(8) Procedures (2)–(7) are successively applied to every axial location from the inlet to the downstream of interest.

Due to the presence of strong coupling between the interface concentration, temperature and evaporation rate, an inner iteration cycle for temperature and concentration equations is introduced in the numerical program. Besides, to check the convergence of the iteration process, the overall mass conservation and the convergence of velocity, temperature and concentration between two consecutive iterations must satisfy the criteria, equations (27) and (28). To

account for the change in liquid film thickness δ in the flow direction due to film evaporation, the finite difference computational grid used must comply with the variations of the liquid and gas computational domains with x. This was accomplished by first locating the interface at a given x-location, and then dividing the gas stream and liquid film regions in the y direction into J and L nodes, respectively. Thus, the interface position was rigorously tracked. This adjustment of grid in the y-direction necessitates numerical interpolation when calculating the convective terms. To further account for the drastic variations of velocity, temperature and concentration in the regions near the inlet and the gas–liquid interface, the grid lines were positioned non-uniformly with the highest grid density being near the inlet and the interface. During the program tests, solutions for a typical case were obtained using different grid sizes to ensure that the solution was grid-independent. It was found in separate numerical calculations that the differences in the local Nusselt number, Nu_x, from computations using either $201 \times 201 \times 81$ or $101 \times 101 \times 41$ grids are always less than 2%. To reduce the cost of computation, the $101 \times 101 \times 41$ grid is chosen for the subsequent computation. To further check the adequacy of the numerical scheme for the present study, results for the limiting case of an extremely thin film thickness are first obtained. Excellent agreement between these present predictions and those of Yan *et al.* [18] and Tsay and Yan [19] was found. In addition, a comparison was also made by comparing the results for the limiting case of mixed convection in a vertical channel without film evaporation with the results of Aung and Worku [5]. The predicted axial variations of wall temperature are indistinguishable from those plotted in Fig. 6 of ref. [5]. Through these program tests, the proposed numerical algorithm is considered to be suitable for the problem.

4. RESULTS AND DISCUSSION

In view of the large number of parameters and of the extreme demands of the computational task, a full parametric exploration is unrealistic. Rather, the parameters were varied systematically in order to examine the key trends in the results. In what follows, results are presented for water and ethanol evaporations. Twelve cases, shown in Table 1, were selected to investigate the effects of liquid film evaporation on mixed convection heat and mass transfer in a vertical channel. In Table 1, the relative humidity of the ambient air ϕ is assigned as 50% for the air–water vapor mixture and 0% for the air–ethanol vapor mixture, which are often encountered in practice. The inlet liquid and mixture are kept at 20°C. All of the cases are based on a vertical channel of width $b = 0.015$ m.

Figures 1–3 show the developments of the axial velocity, temperature and concentration for the water film evaporation under various conditions. For comparison purposes, the results of an extremely thin film thickness are also included in these plots. The velocity profiles develop gradually from the uniform distributions at the inlet to the distorted ones in the downstream region, with maximum velocity shifting toward the insulated wall ($Y = 0$). The shift of the velocity peak results from the film evaporation which causes the flow at the interface to move in the negative y-direction, equation (15). Moreover, the gas mass flow rate continues increasing as the air moves downstream owing to the evaporation of water vapor into the air stream from the liquid film. The distortion in velocity distribution can be made plausible by noting that both the thermal and solutal buoyancies are in the upward direction, opposing the direction of main flow. It is also noted in Fig. 1 that a rise in liquid mass flow rate B would result in a lower axial velocity U. This is attributed to the fact that the larger the liquid mass flow rate B, the lower the gas–liquid interfacial temperature (by checking Fig. 3). Therefore, less water vapor evaporates into the gas stream for a larger liquid flow rate B.

A comparison of the corresponding solid and dashed curves in Fig. 1 indicates that a larger gas mass flow rate is noted by the curves for zero film thickness.

Table 1. Values of major parameters for various cases

Case	T_0 (°C)	q''_w (W m^{-2})	B (kg m^{-1} s^{-1})	Re	Gr_T	Pr	Sc	ϕ (%)
Water film								
I	20	500	0.02	2000	145393.7	0.709	0.597	50
II	20	1000	0.01	2000	290787.5	0.709	0.597	50
III	20	1000	0.02	2000	290787.5	0.709	0.597	50
IV	20	1000	0.04	2000	290787.5	0.709	0.597	50
V	20	3000	0.02	2000	872362.2	0.709	0.597	50
VI	20	1000	0.02	500	290787.5	0.709	0.597	50
VII	20	1000	0.02	1000	290787.5	0.709	0.597	50
Ethanol film								
VIII	20	500	0.04	2000	144498.1	0.710	1.311	0
IX	20	1000	0.01	2000	288996.2	0.710	1.311	0
X	20	1000	0.02	2000	288996.2	0.710	1.311	0
XI	20	1000	0.04	2000	288996.2	0.710	1.311	0
XII	20	3000	0.04	2000	866988.5	0.710	1.311	0

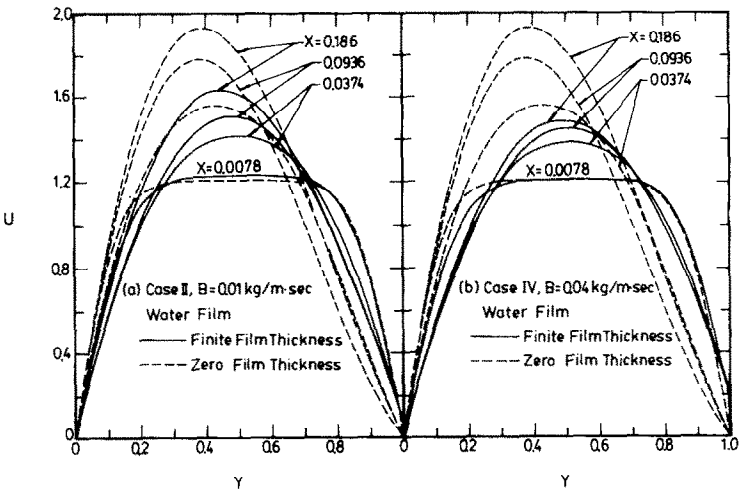

FIG. 1. Developments of axial velocity profiles.

This implies that more water vapor evaporates into the gas stream for cases with zero film thickness. Figures 2(a) and (b) present the axial temperature and mass fraction developments, respectively. It is interesting to observe that both θ and W develop in a very similar fashion. Careful inspection, however, discloses that the concentration boundary layers develop a little more rapidly than the thermal boundary layers. This simply results from the fact that the Prandtl number Pr is slightly larger than the Schmidt number Sc in the gas stream. An overall inspection of Figs. 1 and 2 reveals that the distributions of U, θ and W for zero film thickness resemble those for finite film thickness. Careful observation, however, indicates that the differences between these two treatments (i.e. considering finite film thickness and neglecting film thickness) are substantial, especially in the region close to the gas–liquid interface. Because the interfacial heat and mass transfer characteristics play such an important role in the overall exchange process, the differences in the interfacial heat and mass transfer rates predicted by these two approaches can be rather considerable. In addition, the boundary layers of U, θ and W for zero film thickness develop more rapidly than those for finite film thickness.

Figure 3 shows the distributions of interfacial temperature and mass fraction water vapor along the gas–liquid interface. As expected, the interfacial temperature is higher for a smaller liquid mass flow rate at the same heating condition. Therefore, the corresponding mass fraction is larger for systems with a smaller B. Comparison of the curves of zero film thickness and finite film thickness indicates that the difference between these two treatments increases with the liquid mass flow rate B. This suggests that the assumption of an extremely thin film thickness is a limiting case and is valid only for systems having a small B. For a large liquid mass flow rate B, the assumption of zero film thickness can produce considerable errors.

Figure 4 demonstrates the relative importance of the sensible and latent heat exchanges along the gas–liquid interface. Note that both the sensible and latent heat exchanges increase in the flow direction but decrease with the liquid mass flow rate B. Even at $B = 0.001$ kg m^{-1} s^{-1}, q''_{sl}/q''_{w} is always below 10%, but q''_{ll}/q''_{w} can be above 70%. For a fixed B, q''_{ll} is about

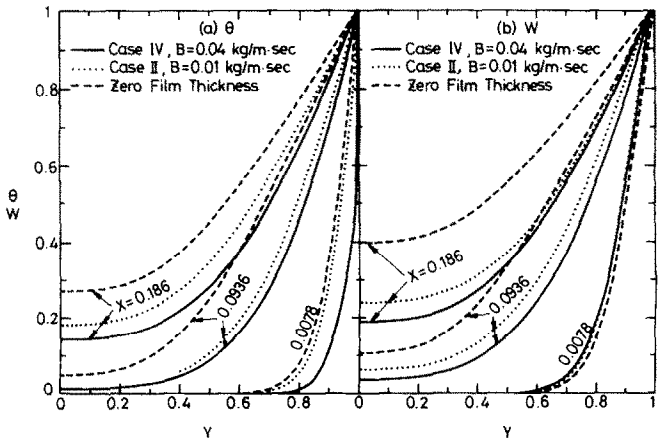

FIG. 2. Developments of axial temperature and mass fraction profiles.

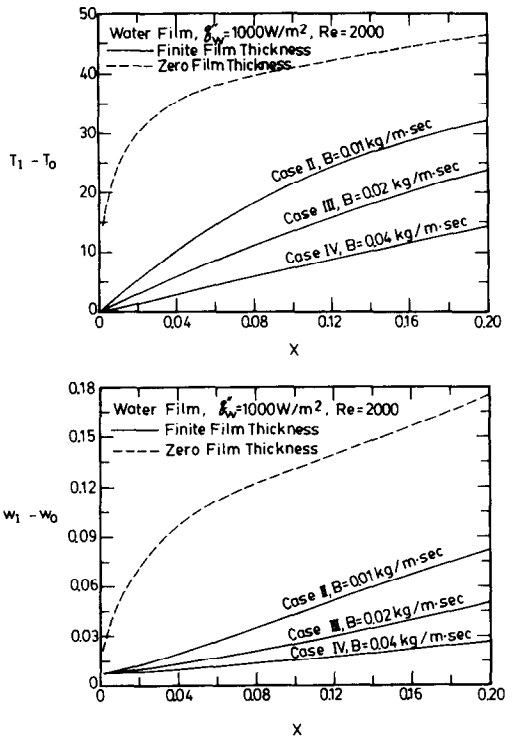

FIG. 3. Axial distributions of interfacial temperature and mass fraction.

five times larger than q''_{sl}. It is also important to point out that the computations with the zero film thickness approximation substantially overpredict the sensible and latent heat transfer at the interface, especially in the entrance region and for large B.

To improve our understanding of the interfacial heat transfer, the variations of the local Nusselt numbers for sensible and latent heat transfer at the interface are shown in Fig. 5 for various B. Regarding Nu_s curves, a larger Nu_s is experienced for a larger liquid flow rate B. This is also observed for Nu_l in Fig. 5(b). It is, however, noted that the actual sensible and latent heat transfer rates shown in Fig. 4 are less effective for larger B. These results clearly indicate that the magnitudes of the Nusselt numbers do not reflect the actual heat transfer rates. The anomaly in the Nusselt numbers defined in equations (22) and (23) results from the larger effect of the liquid mass flow rate on the interface temperature than on q''_{sl} and q''_{ll}, as is evident from Figs. 3 and 4. It is apparent that the magnitude of Nu_l is much larger than that of Nu_s, indicating that interfacial heat transfer resulting from latent heat exchange is much more effective. It is also clearly seen in Fig. 5(a) that the magnitudes of Nu_s are underpredicted in the case where a negligible film thickness is assumed.

It is interesting to investigate the influences of the wall heat flux q''_w and inlet Reynolds number of the gas stream on the interfacial Nusselt number Nu_x. Figure 6(a) shows that near the entrance ($X < 0.04$) a larger Nu_x results for a lower wall heat flux, but as the flow goes downstream ($X > 0.12$) the reverse trend is noted. Of particular interest is the significant increase in Nu_x with X in the downstream region at $q''_w = 3000\ \mathrm{W\ m^{-2}}$. Figure 6(b) shows the effect of Re

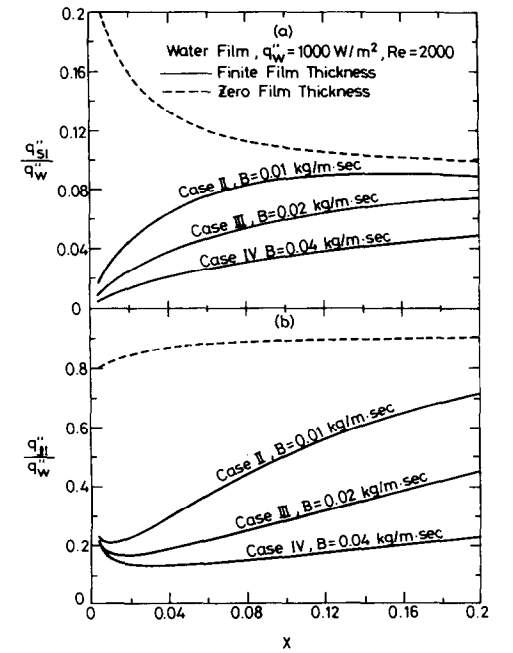

FIG. 4. Distributions of local dimensionless heat transfer rates in the gas side along the channel: (a) interfacial sensible heat flux; (b) interfacial latent heat flux.

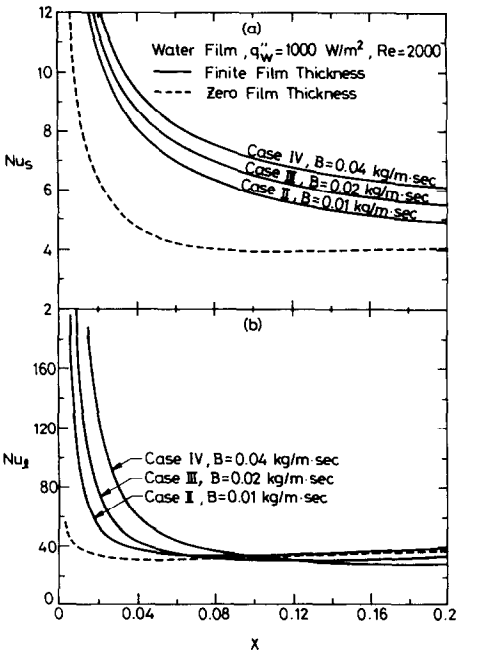

FIG. 5. Effects of liquid mass flow rate on the interfacial Nusselt numbers: (a) sensible heat Nusselt number; (b) latent heat Nusselt number.

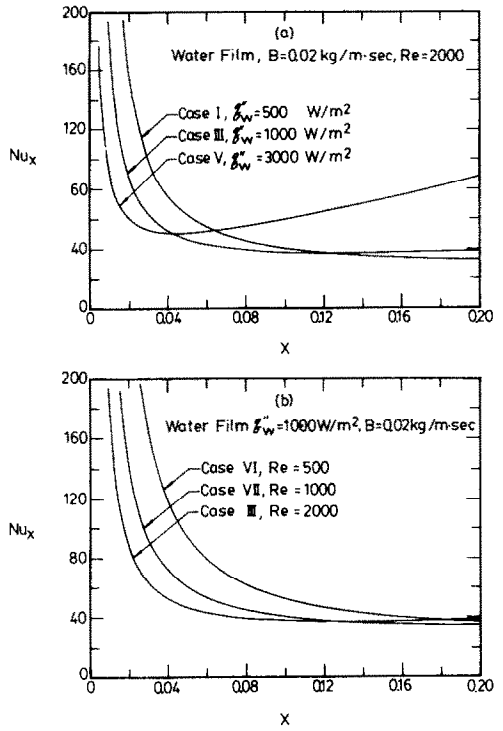

FIG. 6. Effects of wall heat flux q''_w and Reynolds number of gas stream Re on the interfacial Nusselt number Nu_x.

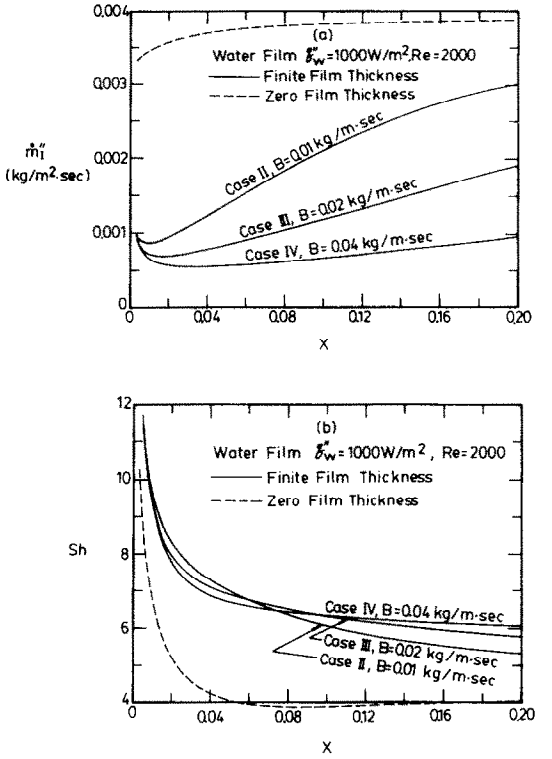

FIG. 7. Effects of liquid mass flow rate B on the interfacial mass evaporation rate and Sherwood number distributions.

on the Nu_x distributions—for $X < 0.12$, Nu_x is larger for a smaller Re. This result is opposite to the usual single phase forced convection heat transfer in channels.

The distributions of the interfacial mass evaporation rate and Sherwood number are presented in Fig. 7 for various B to illustrate the mass transfer characteristics. Similar to the results given in Fig. 4(b) for q''_{ll}/q''_w, a reduction in the film flow rate causes a greater film evaporation and $\dot{m}''_i$ increases with X in the downstream region. These outcomes apparently result from the higher interface temperature T_i at smaller B. T_i increases with X under a uniform flux heating, as shown in Fig. 3(a). The change in the film flow rate has a smaller influence on the Sherwood number variations, as is evident from Fig. 7(b). For $X > 0.1$, the Sherwood number is larger for larger B. It is also noted in Fig. 7 that the analysis neglecting the film thickness overpredicts the mass evaporation rate but underpredicts the Sherwood number.

The effects of the wall heat flux and inlet Reynolds number Re on the mass transfer coefficient are of interest. Figure 8(a) shows that near the entrance a larger Sh results for a system with a larger q''_w. However, downstream the result is reversed. The Sherwood number is only slightly influenced by the change in the Reynolds number (Fig. 8(b)). A larger Re results in a smaller Sh.

As mentioned above, interfacial heat and mass transfer in this wetted wall system are dominated by film vaporization. Therefore, the amount of water

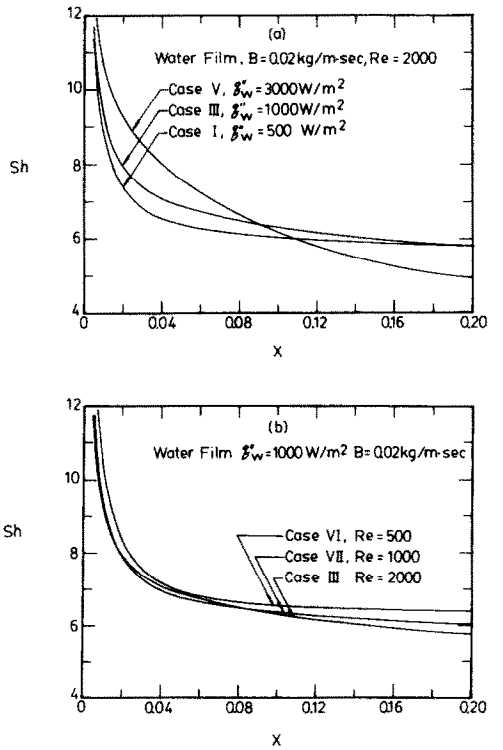

FIG. 8. Effects of wall heat flux q''_w and Reynolds number Re on the variations of Sherwood number Sh.

vapor added to the gas stream due to film vaporization is important in improving our understanding of the heat and mass transfer rates. To quantify the film evaporation a non-dimensional accumulated mass evaporation rate, M_r, is introduced:

$$M_r = \frac{\text{evaporating mass flow rate}}{\text{inlet liquid mass flow rate}} = \int_0^x \dot{m}_l'' \, dx/B. \quad (29)$$

The distributions of M_r for various cases are depicted in Fig. 9. Again, greater film vaporization is found for higher q_w'' and smaller B. It is worth noting that the largest dimensionless accumulated mass evaporation rate at $X = 0.2$ is about 9% for case V.

After examining the mixed convection heat and mass transfer with water film evaporation, attention is turned to the effects of ethanol film evaporation on the interfacial heat and mass transfer. Figure 10(a) shows that a rise in the liquid mass flow rate results in an increase in the local interfacial Nusselt number, Nu_x. For comparison purposes, the predicted results obtained both in the presence and in the absence of a finite liquid film are plotted together. It is clearly seen that the results for zero film thickness underpredicts the interfacial Nusselt number. The influences of q_w'' on Nu_x with ethanol film evaporation are given in Fig. 10(b). Focusing on the curves of $q_w'' = 500$ and 1000 W m^{-2}, it is observed that a larger Nu_x is found for systems with a smaller q_w'', while for $q_w'' = 3000$ W m^{-2}, Nu_x is smallest among these three cases in the region close to the entrance. However, as the flow moves downstream, Nu_x becomes largest for $q_w'' = 3000$ W m^{-2}.

Figure 11 gives the influences of B and q_w'' on the distributions of the Sherwood number. Like the results of water film evaporation, a larger Sh is noted for systems having a larger B. The results in Fig. 11(b) indicate that near the channel entrance a larger Sh is noted for systems with a larger q_w'', while downstream

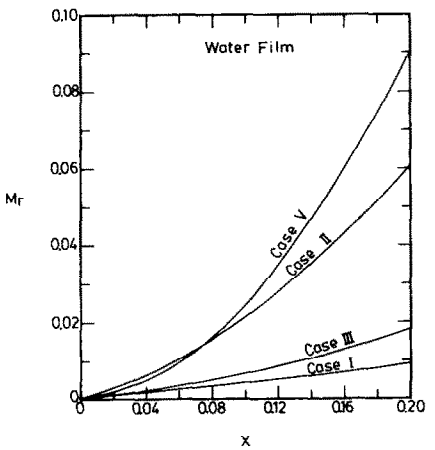

FIG. 9. Distributions of dimensionless accumulated evaporation rate M_r.

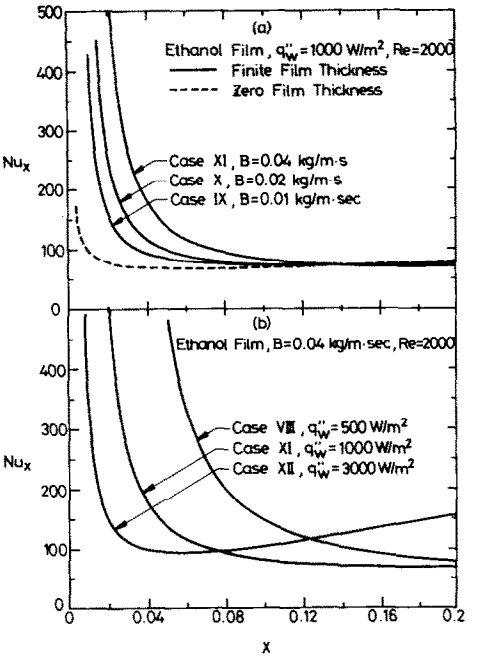

FIG. 10. Effects of liquid mass flow rate and wall heat flux on the interfacial Nusselt number distributions.

Sh becomes smallest for $q_w'' = 3000$ W m^{-2} among the three cases.

5. CONCLUSIONS

The effects of liquid film evaporation on laminar mixed convection heat and mass transfer in a vertical

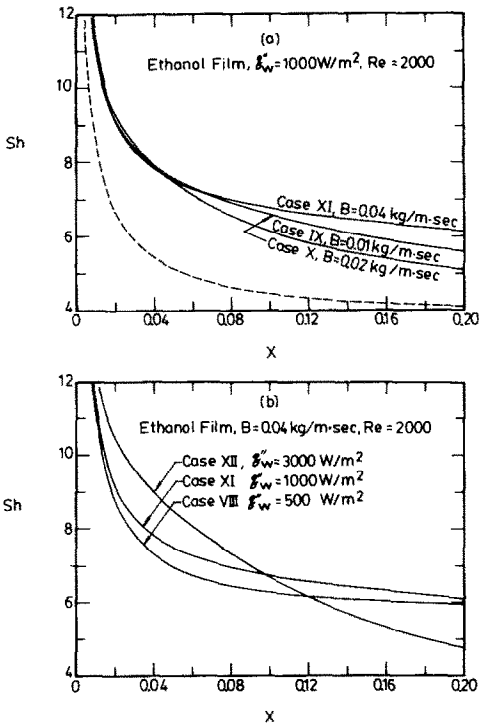

FIG. 11. Effects of liquid flow rate and wall heat flux on Sh distributions.

channel under constant heat flux have been studied. The influences of the thermal condition, inlet liquid mass flow rate and inlet Reynolds number of the gas stream on the momentum, heat and mass transfer in the flow are investigated in great detail. In particular, comparative results are presented for both water and ethanol film evaporations to check the suitability of the assumption of zero film thickness. What follows is a brief summary of the major results.

(1) The liquid film vaporization along the gas–liquid interface dominates the heat and mass transfer. The magnitude of the evaporative latent heat flux may be five times greater than that of sensible heat flux.

(2) The assumption of an extremely thin film thickness is only valid for a low liquid mass flow rate B. However, for a high liquid mass flow rate, the assumption becomes inappropriate, especially near the channel entrance.

(3) The larger the wall heat flux q''_w, the higher the interfacial temperature T_i, which in turn causes a larger latent heat exchange. This is brought about by the larger latent heat transport connected with the greater film evaporation for higher T_i.

(4) A larger mass evaporation rate $\dot{m}''_i$ results for systems with a smaller B, while the reverse is true for the variations of Sherwood number Sh.

It has been realized during the course of the study that when q''_w is well above 3000 W m^{-2}, the upward combined buoyancy forces may result in flow reversal of the gas stream in certain parts of the flow for cases with low Re. Similarly, as the gas stream is pumped upwards, flow reversal may appear in the region near the gas–liquid interface. To handle these situations, a more complicated elliptic flow analysis must be performed. This is a very complex numerical problem and is beyond the scope of the present study. In addition, it is also noted that when the system operates at high gas flow rates, the flowing gas in the channel is turbulent flow. Hence, the results presented in this study, where laminar gas flow is assumed, become invalid. In this connection, it may be worthwhile studying the effects of film evaporation on turbulent mixed convection heat and mass transfer. This will be carried out in the near future.

No experimental work has considered mixed convection heat and mass transfer with film evaporation in the open literature. Therefore, there is no available data with which the numerical results can be compared. However, a similar mathematical model has been used to simulate the natural convection heat and mass transfer in a vertical channel with film evaporation [25]. In ref. [25], comparisons of the numerical results with the experimental data of Yan *et al.* [24] confirmed the adequacy of the mathematical model. This lends support to the employment of the mathematical model proposed for the analysis of the present problem.

Acknowledgement—The support of this research by the Engineering Division of the National Science Council of Taiwan, R.O.C., is greatly appreciated.

REFERENCES

1. B. Zeldin and F. W. Schmidt, Developing flow with combined forced–free convection in an isothermal vertical tube, *J. Heat Transfer* **94,** 211–223 (1972).
2. B. S. Petukhov, A. F. Polyakov and O. G. Martynenko, Buoyancy effect on heat transfer in forced channel flow, Keynote Paper, *7th Int. Heat Transfer Conf.*, Munich, F.R.G., pp. 343–362 (1982).
3. S. Hebchi and S. Acharya, Laminar mixed convection in a symmetrically or asymmetrically heated vertical channel, *Numer. Heat Transfer* **9,** 605–618 (1986).
4. W. Aung and G. Worku, Developing flow and flow reversal in a vertical channel with asymmetric wall temperature, *J. Heat Transfer* **108,** 299–304 (1986).
5. W. Aung and G. Worku, Mixed convection in ducts with asymmetric wall heat flux, *J. Heat Transfer* **109,** 947–951 (1987).
6. B. Gebbhart and L. Pera, The nature of vertical natural convection flows resulting from the combined buoyancy effects of thermal and mass diffusion, *Int. J. Heat Mass Transfer* **14,** 2025–2050 (1971).
7. T. S. Chen and C. F. Yuh, Combined heat and mass transfer in natural convection on inclined surfaces, *Numer. Heat Transfer* **2,** 233–250 (1979).
8. T. S. Chen and C. F. Yuh, Combined heat and mass transfer in natural convection along a vertical cylinder, *Int. J. Heat Mass Transfer* **23,** 451–461 (1979).
9. M. Hason and A. S. Mujumdar, Coupled heat and mass transfer in natural under flux condition along a vertical cone, *Int. Commun. Heat Mass Transfer* **11,** 157–172 (1984).
10. T. S. Lee, P. G. Parikh, A. Acrivos and D. Bershader, Natural convection in a vertical channel with opposing buoyancy forces, *Int. J. Heat Mass Transfer* **25,** 499–511 (1982).
11. C. J. Chang, T. F. Lin and W. M. Yan, Natural convection flows in a vertical open tube resulting from combined buoyancy effects of thermal and mass diffusion, *Int. J. Heat Mass Transfer* **29,** 1453–1552 (1986).
12. W. M. Yan and T. F. Lin, Natural convection heat transfer enhancement through latent heat transfer in vertical parallel plate channel flows, *Can. J. Chem. Engng* **68,** 360–367 (1990).
13. J. Schroppel and F. Thiele, On the calculation of momentum, heat, and mass transfer in laminar and turbulent boundary layer flows along a vaporizing liquid film, *Numer. Heat Transfer* **6,** 475–496 (1983).
14. L. C. Chow and J. N. Chung, Evaporation of water into a laminar stream of air and superheated steam, *Int. J. Heat Mass Transfer* **26,** 373–380 (1983).
15. C. H. Wu, D. C. Davis, J. N. Chung and L. C. Chow, Simulation of wedge-shaped product dehydration using mixtures of superheated steam and air in laminar flow, *Numer. Heat Transfer* **11,** 109–123 (1987).
16. H. M. Yeh, S. W. Tsai and C. C. Yang, Heat and mass transfer in mixed convection over a horizontal plate, *Numer. Heat Transfer* **12,** 229–242 (1987).
17. T. F. Lin, C. J. Chang and W. M. Yan, Analysis of combined buoyancy effects of thermal and mass diffusion on laminar forced convection heat transfer in a vertical tube, *J. Heat Transfer* **110,** 337–344 (1988).
18. W. M. Yan, Y. L. Tsay and T. F. Lin, Simultaneous heat and mass transfer in laminar mixed convection flows between vertical parallel plates with asymmetric heating, *Int. J. Heat Fluid Flow* **10,** 262–269 (1989).
19. H. C. Tsay and W. M. Yan, Binary diffusion and heat transfer in mixed convection channel flow with uniform

heat flux: extremely thin film thickness, *Wärme- und Stoffübertragung* **26,** 23–31 (1990).
20. K. Suzuki, Y. Hagiwara and T. Sato, Heat transfer and flow characteristics of two-component annular flow, *Int. J. Heat Mass Transfer* **26,** 597–605 (1983).
21. T. R. Shembharkar and B. R. Pai, Prediction of film cooling with a liquid coolant, *Int. J. Heat Mass Transfer* **29,** 899–908 (1986).
22. W. W. Baumann and F. Thiele, Heat and mass transfer in evaporating two-component liquid film flow, *Int. J. Heat Mass Transfer* **33,** 267–273 (1990).
23. Y. L. Tsay, T. F. Lin and W. M. Yan, Cooling of falling liquid film through interfacial heat and mass transfer, *Int. J. Multiphase Flow* **16,** 853–865 (1990).
24. W. M. Yan, T. F. Lin and Y. L. Tsay, Evaporative cooling of liquid film through interfacial heat and mass transfer in a vertical channel—I. Experimental study, *Int. J. Heat Mass Transfer* **34,** 1105–1111 (1991).
25. W. M. Yan and T. F. Lin, Evaporative cooling of liquid film through interfacial heat and mass transfer in a vertical channel—II. Numerical study, *Int. J. Heat Mass Transfer* **34,** 1113–1124 (1991).
26. E. R. G. Eckert and R. M. Drake, Jr., *Analysis of Heat and Mass Transfer*, Chaps 20 and 22. McGraw-Hill, New York (1972).
27. R. B. Bird, W. E. Steward and E. N. Lightfood, *Transport Phenomena*. Wiley, New York (1960).
28. T. Fujii, Y. Kato and K. Mihara, Expressions of transport and thermodynamic properties of air, steam and water, Sei San Ka Gaku Ken Kyu Jo, Report No. 66, Kyu Shu Dai Gaku, Kyu Shu, Japan (1977).
29. *JSME Data: Thermophysical Properties of Fluids*. The Japan Society of Mechanical Engineers (1983).
30. S. V. Patankar, *Numerical Heat Transfer and Fluid Flow*, Chap. 4. Hemisphere/McGraw-Hill, New York (1980).